9. K. A. Zemski *et al.*, *Chem. Rev.* **111**, 6491–6512 (2011).
10. A. Römpp *et al.*, *Angew. Chem. Int. Ed.* **49**, 3834–3838 (2010).
11. A. Zavalin *et al.*, *J. Mass Spectrom.* **47**, 1473–1481 (2012).
12. J. L. Norris, R. M. Caprioli, *Chem. Rev.* **113**, 2309–2342 (2013).
13. E. J. Lanni, S. S. Rubakhin, J. V. Sweedler, *J. Proteomics* **75**, 5036–5051 (2012).
14. B. Spengler, *Anal. Chem.* **87**, 64–82 (2015).
15. R. Knochenmuss, L. V. Zhigilei, *Anal. Bioanal. Chem.* **402**, 2511–2519 (2012).
16. K. Dreisewerd, M. Schürenberg, M. Karas, F. Hillenkamp, *Int. J. Mass Spectrom. Ion Process.* **141**, 127–148 (1995).
17. J. Schiller *et al.*, *Prog. Lipid Res.* **43**, 449–488 (2004).
18. K. Dreisewerd, *Anal. Bioanal. Chem.* **406**, 2261–2278 (2014).
19. L. Hanley, R. Zimmermann, *Anal. Chem.* **81**, 4174–4182 (2009).
20. C. H. Becker, K. J. Wu, *J. Am. Soc. Mass Spectrom.* **6**, 883–888 (1995).
21. P. Nemes, A. Vertes, *Anal. Chem.* **79**, 8098–8106 (2007).
22. J. Soltwisch, J. Souady, S. Berkenkamp, K. Dreisewerd, *Anal. Chem.* **81**, 2921–2934 (2009).
23. H. Kettling *et al.*, *Anal. Chem.* **86**, 7798–7805 (2014).
24. A. Rohlfing, A. Leisner, F. Hillenkamp, K. Dreisewerd, *J. Chem. Phys. C* **114**, 5367–5381 (2010).
25. Further experimental details can be found in the supplementary online materials.
26. J. Y. Zhang, D. S. Nagra, L. Li, *Anal. Chem.* **63**, 2995–2999 (1991).
27. Q. Lin, R. Knochenmuss, *Rapid Commun. Mass Spectrom.* **15**, 1422–1426 (2001).
28. J. Soltwisch, T. W. Jaskolla, F. Hillenkamp, M. Karas, K. Dreisewerd, *Anal. Chem.* **84**, 6567–6576 (2012).
29. A. N. Krutchinsky, B. T. Chait, *J. Am. Soc. Mass Spectrom.* **13**, 129–134 (2002).

ACKNOWLEDGMENTS

We thank Waters Corp. and GWU Lasertechnik for technical support; F. Spieker and J. Haier for animal tissue; J. Klingauf for scanning electron microscopy images; W. Kramer for Fig. 1; and S. Albrecht, H. Karch, T. Kuhlmann, G. Pohlentz, and J. Y. Yew for helpful discussions. Financial support by the German Science Foundation (grants DR416/8-2 and DR416/9-1 to K.D., SO976/2-1 to J.S., GRK 1409 and MU845/4-2 to J.M.) and the Interdisciplinary Center for Clinical Research (IZKF) Münster (Z03 to K.D.) is gratefully acknowledged. We dedicate this work to the memory of Dr. Franz Hillenkamp in recognition of his lifetime achievements in the field of MALDI mass spectrometry.

SUPPLEMENTARY MATERIALS

www.sciencemag.org/content/348/6231/211/suppl/DC1
Materials and Methods
Figs. S1 to S9
Tables S1 to S3
References (*30*–*39*)

17 October 2014; accepted 23 February 2015
Published online 5 March 2015;
10.1126/science.aaa1051

QUANTUM COMPUTING

Quantum versus classical annealing of Ising spin glasses

Bettina Heim,[1] Troels F. Rønnow,[1] Sergei V. Isakov,[2] Matthias Troyer[1]*

Quantum annealers use quantum fluctuations to escape local minima and find low-energy configurations of a physical system. Strong evidence for superiority of quantum annealing (QA) has come from comparing QA implemented through quantum Monte Carlo (QMC) simulations to classical annealing. Motivated by recent experiments, we revisit the question of when quantum speedup may be expected. Although a better scaling is seen for QA in two-dimensional Ising spin glasses, this advantage is due to time discretization artifacts and measurements that are not possible on a physical quantum annealer. Simulations in the physically relevant continuous time limit, on the other hand, do not show superiority. Our results imply that care must be taken when using QMC simulations to assess the potential for quantum speedup.

With the first archaeological records dating back more than 6000 years (*1*), thermal annealing is likely to be the oldest optimization method in human history. First heating a material and then letting it cool down slowly can relieve internal stresses and allow the material to achieve a lower-energy state. Inspired by thermal annealing, the simulated annealing (SA) algorithm (*2*) was proposed to find the ground states of combinatorial optimization problems—in particular, Ising spin glasses described by the Hamiltonian

$$H_c = -\sum_{i<j} J_{ij} s_i s_j - \sum_i h_i s_i \qquad (1)$$

Here, the N spins s_i can take the values ±1. Spins s_i and s_j on lattice sites i and j are coupled by the Ising term J_{ij}, and the h_i are local fields. Nonconvex optimization problems—such as finding the ground state of this Ising spin glass (*3*), job scheduling (*4*), circuit minimization (*5*), and chain optimization (*6*)—find applications in many areas. These problems are all nondeterministic polynomially complete (*7*), which implies polynomial time mapping from one problem to the other. Thus, any method to efficiently find solutions to the Ising spin glass problem would provide an efficient way of solving other important problems.

Applying the Metropolis algorithm (*8*), Kirkpatrick *et al.* demonstrated that using SA—i.e., simulating the process of cooling Ising spin glasses in a Monte Carlo simulation—is an excellent method to minimize H_c (*2*). Starting in a random state at high temperature, the system is slowly cooled. Thermal excitations allow the escape from local minima and relaxation into a low-energy state with energy equal or near that of the ground state E_0 (*9*). We will refer to the difference between the final energy E and E_0 as the residual energy $E_{res} = E - E_0$. Quantum annealing (QA) (*10*–*14*) uses quantum tunneling instead of thermal excitations to escape from local minima, which can be advantageous in systems with tall but narrow barriers, which are easier to tunnel through than to thermally climb over. To perform QA of Ising spin glasses, an additional kinetic term is added, usually by applying a transverse magnetic field. The time-dependent Hamiltonian of QA is given by

$$H_q = -\sum_{i<j} J_{ij}\sigma_i^z\sigma_j^z - \sum_i h_i\sigma_i^z - \Gamma(t)\sum_i \sigma_i^x \qquad (2)$$

where σ_i^z and σ_i^x are Pauli z and x operators, respectively. The transverse field $\Gamma(t)$ is initially much larger then the couplings, $\Gamma(0) \gg |J_{ij}|, |h_i|$, and the spins start out aligned in the x direction. $\Gamma(t)$ is slowly reduced to zero such that at the end of the annealing process, we recover the Hamiltonian of the initial Ising spin glass problem. On a perfectly coherent quantum device, this algorithm (*13*) would find the ground state of the spin glass in question with high probability, provided that the annealing time t_a is sufficiently long to stay adiabatically in the ground

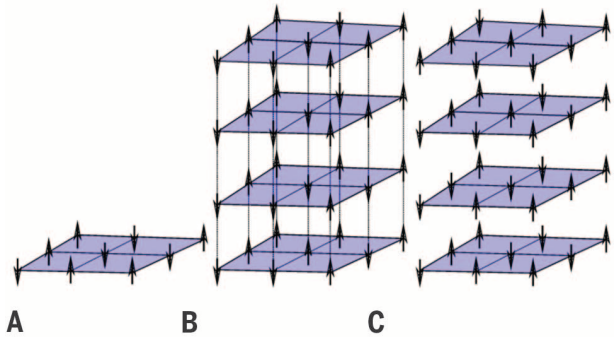

Fig. 1. Illustration of computational resources used in SA and DT-SQA. (**A**) A lattice of classical spins used in SA. (**B**) DT-SQA maps the transverse field Ising model to a classical system representing imaginary time paths of the quantum spins in an additional imaginary time direction. We show an example of $M = 4$ time slices with discrete time steps $\Delta\tau = \beta/M$. (**C**) With similar computational effort, we can perform SA on M independent replicas.

[1]Theoretische Physik, ETH Zurich, 8093 Zurich, Switzerland. [2]Google, Brandschenkestrasse 110, 8002 Zurich, Switzerland.
*Corresponding author. E-mail: troyer@phys.ethz.ch

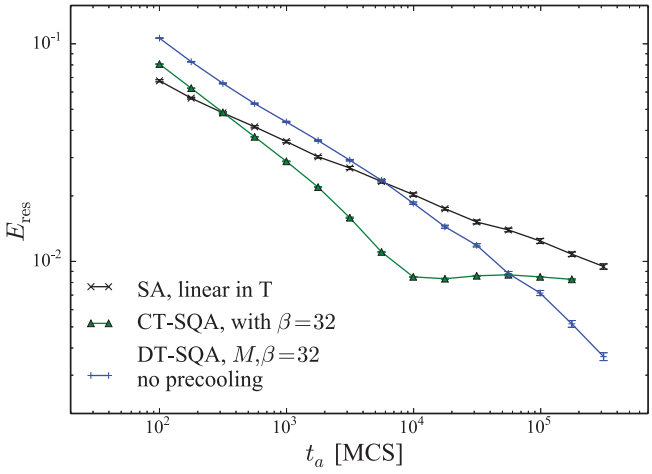

Fig. 2. Residual energy E_{res} dependence as a function of annealing time t_a. Graph shows the residual energy for SA, DT-SQA, and CT-SQA for the square-lattice Ising spin glass instance of (*19*) with 6400 spins. The annealing time is in units of MCS, corresponding to one attempted update per spin. E_{res} and error bars (indicating 1-σ statistical error) are obtained by averaging over 40 annealing runs.

state (*15*, *16*). QA can also be performed at nonzero temperature—for example, on spin glass materials (*17*) or in programmable devices (*18*).

Although the simulation of unitary time evolution scales exponentially with N, a variant of QA can be efficiently performed on a classical computer using stochastic dynamics in a quantum Monte Carlo (QMC) simulation (*19*, *20*). In this simulated quantum annealing (SQA) algorithm, the partition function of the quantum Ising model in a transverse field is mapped to that of a classical Ising model in one higher dimension corresponding to the imaginary time direction (*21*), as shown in Fig. 1. Details of the algorithms are discussed in the supplementary materials (*22*).

Strong evidence for QA being superior to classical annealing comes from a comparison of the performance of SQA and SA (*14*, *19*, *20*). Upon increasing the annealing time, the residual energy in a two-dimensional (2D) Ising spin glass was seen to drop faster in SQA than in SA, indicating that quantum tunneling may be advantageous in finding low-energy states. However, recent studies of the performance of D-Wave devices (D-Wave Systems, Burnaby, Canada), which are designed to use superconducting circuits to realize QA, failed to demonstrate indications of quantum speedup (*23*). Furthermore, in contrast to the work in (*19*, *20*), no advantage of SQA over SA was observed.

To understand these contradictory findings, we first confirm the results of Santoro *et al.* (*19*) by observing better scaling of SQA compared with SA in Fig. 2 [and in more detail in fig. S1 in (*22*)]. However, these simulations were performed with a small number of time slices M and a corresponding large time step $\Delta\tau = \beta/M = 1$, which we refer to as a discrete time SQA (DT-SQA) simulation. Here, $\beta = 1/k_BT$ (k_B, Boltzmann's constant; T, temperature) is the inverse temperature. Discrete time steps incur time discretization errors of order $\mathcal{O}(\beta^3/M^2)$. To obtain accurate thermal averages for the quantum system, one needs to extrapolate results to $\Delta\tau \to 0$ or perform a continuous time simulation (CT-SQA) that works directly in the limit $\Delta\tau \to 0$ (*24*).

Repeating the simulations using CT-SQA, we see an entirely different behavior. Although the performance is improved for short t_a, the residual energy saturates for longer t_a at a level higher than that reached by SA. Whereas the time discretization error in DT-SQA does not affect its use as a classical optimization algorithm, it does not reflect a physical quantum system, for which the continuous time limit is relevant. Hence, the circumstances under which SQA outperforms SA depend on whether we use SQA as a quantum-inspired classical algorithm or as simulation of a physical system.

Understanding the role of time discretization in SQA is important both to estimate the performance of experimental quantum annealers as well as to tune SQA as a classical optimization algorithm. To achieve this, we went beyond the single instance of (*19*) and studied 1000 random spin glass instances on an 80-by-80 square lattice with periodic boundary conditions. We use the same distribution of uniform couplings $J_{ij} \in (-2, 2)$ and $h_i = 0$. The exact ground-state energies E_0 are obtained using the spin glass server (*25*).

In Fig. 3A, we show E_{res} as a function of t_a for various M. As expected, for $M \to \infty$, DT-SQA converges toward the continuous time limit. We confirm the behavior already indicated in Fig. 2: Although the initial scaling is better in CT-SQA, lower residual energies are reached using a large time step. Comparing $M = 16$ and 64, a lower residual energy of $2 \cdot 10^{-3}$ is found for $M = 16$ compared with $5 \cdot 10^{-3}$ for $M = 64$, despite the computational effort being four times smaller.

Analyzing the residual energies as a function of temperature with a constant number of time slices in Fig. 3B leads to a similar observation. For $\beta < 20$, the DT-SQA results match well with the CT-SQA results [shown in fig. S4 in (*22*)], indicating that $M = 64$ is sufficient to converge to the continuous time limit. At lower temperatures, deviations from CT-SQA are seen, and the larger $\Delta\tau = \beta/M$ allows us to find states with lower energy than in CT-SQA.

When using SQA as a classical optimization algorithm, we can search the final configuration for the time slice with the lowest energy instead of averaging over all time slices. However, we also have to take into consideration the increased computational effort of QMC simulations compared with SA and multiply the number of Monte Carlo steps (MCS) by M for DT-SQA and by β for CT-SQA. Plotting the residual energy as a function of total computational effort in Fig. 4A, we find that with suitable chosen β and M, DT-SQA outperforms SA, agreeing with (*19*).

To use SQA as a classical optimization algorithm, it is thus advantageous to use a small $\Delta\tau$ for short t_a, because the continuous time limit has a more rapid initial decrease of E_{res}. When annealing for longer t_a, a lower temperature and larger $\Delta\tau$ are preferred to reach lower asymptotic residual energies. To reach the lowest energies, rather large $\Delta\tau$ values of order unity are needed, where the system consists of few moderately coupled individual replicas instead of a more tightly coupled continuous path of configurations.

Simulated quantum annealing simulations can escape a local minimum through path-integral configurations corresponding to tunneling events. These configurations spend only short (imaginary) times in high-energy configurations on the barrier, thus avoiding the full cost of the barrier. Although the Monte Carlo dynamics in SQA is different from unitary dynamics of QA, they both use a form of quantum tunneling to escape local minima and are thus similarly sensitive to the nature of barriers. Hence, SQA may indicate whether a physical QA device is expected to show an advantage over SA. A good correlation of SQA [and a mean-field version thereof (*26*)] has been seen for spin glass problems on a D-Wave One device (*27*).

To use SQA to predict where QA might outperform SA, we have to take the physical continuous time limit and use either CT-SQA or DT-SQA with large enough M. Figure 4B shows the slightly higher residual energy obtained this way. For short t_a up to $t_a = 10^5$ MCS, SQA still outperforms SA when choosing an appropriate temperature, but the asymptotic scaling is better for SA.

In all of our simulations, the residual energy saturates at some point in SQA but not in SA, indicating that the simulations consistently get stuck in local minima for SQA. This may be understood by the more deterministic dynamics of QA, which prefers a subset of low-energy states (*28*). Repeating SQA, one may thus get consistently stuck in similar local minima. SA, on the other hand, starts in a random state at high temperatures and therefore explores the configuration space more evenly. The more deterministic nature of SQA also explains the counterintuitive result that for some choices of parameters (see Fig. 4), the E_{res} may increase when annealing more slowly. Similar to the work in (*29*), perturbing a quantum annealer (for example, by annealing faster) can excite a system out of a local minimum and thus help to ultimately uncover a better solution.

Reinvestigating evidence for QA outperforming classical annealing for spin glass instances, we thus find that the performance advantage previously observed for path-integral QMC annealing compared with SA for 2D spin glasses (*19*, *20*) is

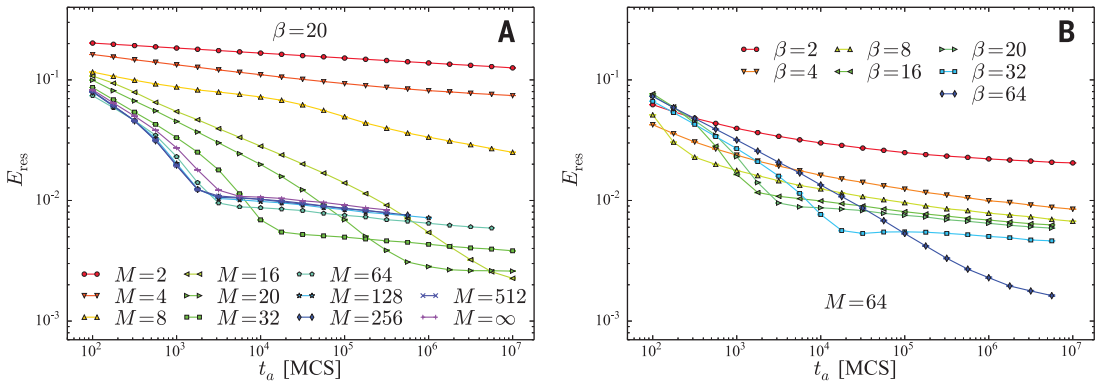

Fig. 3. Convergence and temperature dependence of SQA. (**A**) Convergence of DT-SQA toward the continuous time limit $M = \infty$ obtained by CT-SQA. Shown is the average of 1000 different disorder realizations annealed at an inverse temperature of $\beta = 20$. The lowest-energy configuration along the imaginary time axis was taken to calculate the residual energy. (**B**) Temperature dependence of DT-SQA with a constant number of $M = 64$ time slices. Lowering the temperature increases the time step $\Delta\tau = \beta/M$. This reduces the initial drop in energy but allows us to ultimately find a final configuration with lower energy.

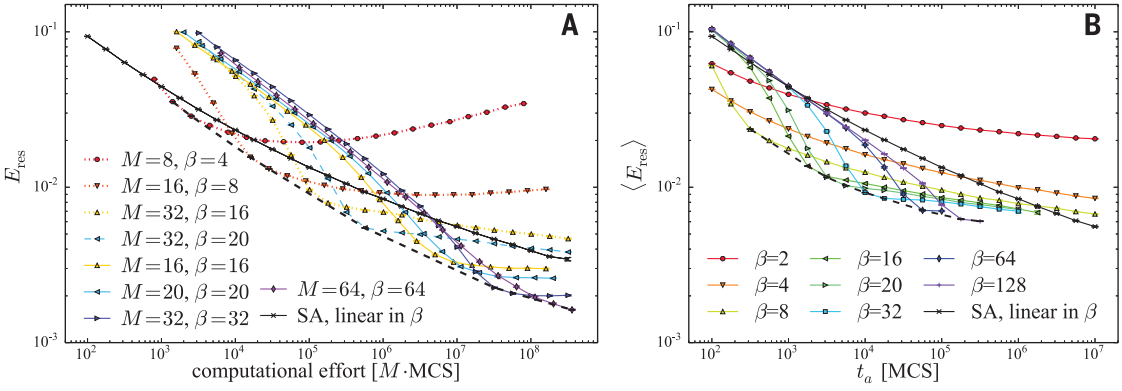

Fig. 4. Performance of SQA as a classical optimizer versus a physical system. (**A**) SQA as a classical optimizer: When choosing a suitable annealing temperature and time step, DT-SQA scales better than SA, consistent with the results of (*19*). (**B**) SQA as a simulation of a physical system, using large enough M to be converged to the continuous time limit. Here we average the final energy over imaginary time instead of picking the lowest-energy configuration.

due to large imaginary time steps in the path integral and choosing the lowest energy over all time slices. When taking the limit of continuous time and measuring the average energy, the advantage vanishes. These results are also consistent with recent arguments that 2D spin glasses should not see any quantum speedup in QA (*30*). It will now be important to explore whether 3D spin glasses or spin glasses with long-range couplings, where barriers are taller than in 2D, show superiority for QA. There, and for problem instances derived from hard application problems, it will once more be essential to investigate both discrete and continuous time simulations. CT-QMC simulations can estimate the potential of QA to outperform SA, but ultimately the unitary dynamics of QA will need to help it outperform DT-SQA, which is by itself an efficient classical optimization algorithm. Although the answer to this question will have to wait for experiments on improved QA devices, SQA simulations performed in the correct way can guide the design of these future experiments.

REFERENCES AND NOTES

1. M. Radivojević, T. Rehren, J. Kuzmanović-Cvetković, M. Jovanović, J. P. Northover, *Antiquity* **87**, 1030–1045 (2013).
2. S. Kirkpatrick, C. D. Gelatt Jr., M. P. Vecchi, *Science* **220**, 671–680 (1983).
3. F. Barahona, *J. Phys. Math. Gen.* **15**, 3241–3253 (1982).
4. R. Graham, *Bell Syst. Tech. J.* **45**, 1563–1581 (1966).
5. D. E. Knuth, *The Art of Computer Programming, Volume 4, Fascicle 1: Bitwise Tricks & Techniques; Binary Decision Diagrams* (Addison-Wesley Professional, Boston, ed. 12, 2009).
6. L.-P. Wong, M. Y.-H. Low, C. S. Chong, *Int. J. Artif. Intell. Tools* **19**, 305–334 (2010).
7. S. A. Cook, in *Proceedings of the Third Annual ACM Symposium on Theory of Computing* (Association for Computing Machinery, New York, 1971), pp. 151–158.
8. N. Metropolis, A. W. Rosenbluth, M. N. Rosenbluth, A. H. Teller, E. Teller, *J. Chem. Phys.* **21**, 1087–1092 (1953).
9. D. Bertsimas, J. Tsitsiklis, *Stat. Sci.* **8**, 10–15 (1993).
10. P. Ray, B. K. Chakrabarti, A. Chakrabarti, *Phys. Rev. B* **39**, 11828–11832 (1989).
11. A. B. Finnila, M. A. Gomez, C. Sebenik, C. Stenson, J. D. Doll, *Chem. Phys. Lett.* **219**, 343–348 (1994).
12. T. Kadowaki, H. Nishimori, *Phys. Rev. E Stat. Phys. Plasmas Fluids Relat. Interdiscip. Topics* **58**, 5355–5363 (1998).
13. E. Farhi *et al.*, *Science* **292**, 472–475 (2001).
14. A. Das, B. K. Chakrabarti, *Rev. Mod. Phys.* **80**, 1061–1081 (2008).
15. L. Landau, *Phys. Z. Sowjetunion* **2**, 46–51 (1932).
16. C. Zener, *Proc. R. Soc. London Ser. A* **137**, 696–702 (1932).
17. J. Brooke, D. Bitko, T. F. Rosenbaum, G. Aeppli, *Science* **284**, 779–781 (1999).
18. M. W. Johnson *et al.*, *Nature* **473**, 194–198 (2011).
19. G. E. Santoro, R. Martonák, E. Tosatti, R. Car, *Science* **295**, 2427–2430 (2002).
20. R. Martoňák, G. E. Santoro, E. Tosatti, *Phys. Rev. B* **66**, 094203 (2002).
21. M. Suzuki, *Prog. Theor. Phys.* **56**, 1454–1469 (1976).
22. See the supplementary materials on *Science* Online.
23. T. F. Rønnow *et al.*, *Science* **345**, 420–424 (2014).
24. H. Rieger, N. Kawashima, *Eur. Phys. J. B* **9**, 233–236 (1999).
25. www.informatik.uni-koeln.de/spinglass/.
26. S. W. Shin, G. Smith, J. A. Smolin, U. Vazirani, http://arxiv.org/abs/1401.7087 (2014).
27. S. Boixo *et al.*, *Nat. Phys.* **10**, 218–224 (2014).
28. Y. Matsuda, H. Nishimori, H. G. Katzgraber, *New J. Phys.* **11**, 073021 (2009).
29. E. Crosson, E. Farhi, C. Y.-Y. Lin, H.-H. Lin, P. Shor, http://arxiv.org/abs/1401.7320 (2014).
30. H. G. Katzgraber, F. Hamze, R. S. Andrist, *Phys. Rev. X* **4**, 021008 (2014).

ACKNOWLEDGMENTS

We thank H. G. Katzgraber, G. Santoro, and I. Zintchenko for useful discussions and G. Santoro for providing the spin glass instance used in (*19*). This work was supported by the Swiss National Science Foundation through the National Competence Center in Research QSIT and by the European Research Council (ERC) through ERC Advanced Grant SIMCOFE. M.T. acknowledges the hospitality of the Aspen Center for Physics, supported by NSF grant 1066293. The spin glass server (*25*) was used to obtain the ground states for our problem instances. The original data used to create the figures can be obtained from the corresponding author.

SUPPLEMENTARY MATERIALS

www.sciencemag.org/content/348/6231/215/suppl/DC1
Materials and Methods
Fig. S1 to S4
References (*31*–*34*)

3 December 2014; accepted 26 February 2015
Published online 12 March 2015;
10.1126/science.aaa4170

Quantum versus classical annealing of Ising spin glasses

Bettina Heim *et al.*

Science **348**, 215 (2015);
DOI: 10.1126/science.aaa4170

Science (print ISSN 0036-8075; online ISSN 1095-9203) is published weekly, except the last week in December, by the American Association for the Advancement of Science, 1200 New York Avenue NW, Washington, DC 20005.